ResearchGate

See discussions, stats, and author profiles for this publication at: https://www.researchgate.net/publication/260342970

Bare Earth LiDAR to Gridded Topography for the Pascagoula River, MS: An Accuracy Assessment

Article · March 2014

DOI: 10.1061/9780784412411.00018

CITATION
1

READS
61

3 authors, including:

Matthew V. Bilskie
Louisiana State University
32 PUBLICATIONS **204** CITATIONS
SEE PROFILE

Reza Akhavian
California State University, East Bay
20 PUBLICATIONS **114** CITATIONS
SEE PROFILE

All content following this page was uploaded by Matthew V. Bilskie on 02 April 2014.

The user has requested enhancement of the downloaded file.

Bare Earth LiDAR to Gridded Topography for the Pascagoula River, MS: An Accuracy Assessment

Matthew V. Bilskie[1], Reza Akhavian[2], and Scott Hagen[3]

[1] Contact person. University of Central Florida, Department of Civil, Environmental, and Construction Engineering, P.O. Box 162450, Orlando, FL, 32816, USA. Phone: +1-407-823-1176. E-mail: Matt.Bilskie@gmail.com

[2] University of Central Florida, Department of Civil, Environmental, and Construction Engineering, P.O. Box 162450, Orlando, FL, 32816, USA. Phone: +1-979-587-3134. E-mail: reza.akhavian@gmail.com

[3] University of Central Florida, Department of Civil, Environmental, and Construction Engineering, P.O. Box 162450, Orlando, FL, 32816, USA. Phone: +1-407-823-3903. E-mail: scott.hagen@ucf.edu.

ABSTRACT

This paper investigates the development of an optimal bare-earth LiDAR-derived digital elevation model for use in a shallow water equations model for a portion of the Pascagoula River Basin (coastal Mississippi). It is vital to represent the floodplain topography as accurately as possible since terrain is the first factor that can promote or inhibit water flow. An essential step is processing the dense LiDAR points to a DEM or FEM; however it is crucial that the correct interpolation scheme and grid size is employed for an efficient and accurate terrain representation. In the presented research several DEMs and FEMs were developed and three interpolation routines were tested. Three paths for interpolation were considered and elevation error was computed for each: 1) LiDAR to DEM; 2) LiDAR to FEM; and 3) LiDAR to DEM to FEM. The error of each interpolation scheme is assessed in terms of root mean square error and a relationship between DEM grid size and finite element mesh size was found. This paper aims to determine the most appropriate and efficient interpolation routine and grid size for this region for use in a two-dimensional shallow water equations model.

1. INTRODUCTION

Accurate, high resolution LiDAR (Light Detection and Ranging) data is becoming more accessible in the coastal United States, mainly for flood protection studies. Also, much effort has been put forth in the area of finite element numerical modeling of astronomical tides and hurricane storm surge for understanding the physical processes that occur across large and small scales, (Lynch, 1983; Westerink *et al.*, 1992; Blain *et al.*, 1994; Westerink *et al.*, 1994; Dietsche *et al.*, 2007; Bacopoulos, 2009; Bunya *et al.*, 2010). As computer technology advances, especially in the realm of parallel computing, these numerical models can begin to cover broad

geographical bounds at high temporal and spatial resolutions. Efficiently merging high density bare earth LiDAR with high resolution hydrodynamic models can generate further understanding of the physical processes in coastal waters leading to more accurate astronomic tide and storm surge prediction. Therefore, it is of importance to represent above water (terrain) elevation correctly and accurately in storm surge inundation models (Coggin, 2011).

With the advancement of LiDAR acquisition and processing, much has been published on bare earth derived digital elevation models (DEM) to show how the interpolation scheme and grid size affect the overall accuracy. Interpolation of irregularly spaced LiDAR points is needed to generate a regular DEM that provides a better representation of the land surface (Lloyd & Atkinson, 2002; Anderson *et al.*, 2005). Interpolation is often defined as the procedure to estimate values at unknown locations based on values at sampled locations (Ali, 2004). Interpolation is a fundamental step in terrain processing, however differing opinions exist in literature for the best and most efficient algorithm (Li *et al.*, 2005; Maune, 2007). The accuracy of the interpolation is largely dependent on the properties of the surface, density and spacing of control points, and on the interpolation function itself (Kubik & Botman, 1976).

Lloyd (2002) employed inverse distance weighted (IDW), ordinary kriging (OK) and kriging with a trend model (KT) to an area of varying hillslope topography to create a digital surface model (DSM) from LiDAR data. It was found that IDW produced the largest error, but resulted in a lower standard deviation than other interpolation schemes. In areas where point densities were low, OK and KT provided the most accurate predictions, but no advantage existed when the point density was high.

Ali (2004) found that IDW produced the most realistic and accurate cross-section profiles compared to kriging and triangular irregular network (TIN) interpolation based on the very important point algorithm (VIP). Also, inverse distance produced similar results to the TIN method except in terms of random error where single locations were considered. Ali concluded that kriging should not be used for terrain models based on LiDAR.

Anderson *et al.* (2005) found IDW as the most sufficient interpolation function for creating a DEM from irregularly spaced LiDAR from a root mean square error (RMSE) and mean square error approach. Su and Broke (2006) employed a similar technique to that of Anderson *et al.* (2005) and also found IDW to be more efficient, than that of spline and kriging.

Bater *et al.* (2009) tested seven interpolation functions and assessed them in terms of RMSE by randomly selecting prediction 97% of the LiDAR points for DEM generation and using the remaining 3% to check the accuracy. Linear and natural neighbor (NN) interpolation performed the best in terms of overall error. Bater also indicated that spatial resolution of the DEM is just as important as the interpolating function. "Determination of a DEM grid size is the central problem for DEM generation and analysis" (p. 40) (Liu, 2008).

When interpolating irregularly spaced points, it is common to produce a DEM at regularly spaced intervals. These regularly spaced intervals are termed DEM grid cells, where the value of the cell represents the terrain surface, a numeric value of

elevation, across the entire cell (Maune, 2007). The resolution of the DEM is that of the regular spacing interval between the grid cell centers. In terrain modeling, it is important to utilize a DEM grid size that represents the land surface well, while also having a large enough resolution to allow efficient data storage and a level of particular accuracy (Gao, 1997). It is intuitive that as the DEM grid size becomes coarser the terrain representation will be degraded, and vice versa (Kienzle, 2004). Typically, DEM grid size should not be higher than that of the source data (Florinksy, 1998); however using a dense terrain dataset to develop a coarse resolution DEM will make poor use of the high resolution source data (Liu, 2008). An appropriate grid size is a function of many items including but not limited to source data density, complexity of the surface, and the application (Liu, 2008).

Hengl (2006) linked terrain grid resolution with that of digital signal processing. Similarities exist between digital signal reconstruction and construction of a DEM that discretizes a 3D function of the terrain surface. According to the Shannon-Nyquist sampling theorem (Shannon, 1949), a continuous function can be reconstructed from a discrete function (sampled data) if the sampling rate exceeds two times the maximum frequency. In other words, if two samples per the shortest wavelength are collected, then the continuous function can be recomposed from the set of sampled data (Florinksy, 2002). Using this rule, Hengl stated the cell resolution should be at least half the average spacing between inflection points along a cross section:

$$p \le \frac{l}{2 \bullet n(\delta z)} \tag{1}$$

where p = recommended point spacing, l = length of cross-section transect and $n(\delta z)$= number of inflection points measured. For example, if 20 points are measured (i.e. inflection points) with an average spacing of 0.8 meters, Equation (1) yields a grid size of 0.4 meters. However, the smallest distance found between all points should be the minimum limit to grid resolution (Hengl, 2006).

Figure 1 depicts a plot of a continuous surface with measurements taken at random distance intervals along a transect. The gray bars represent resampling the data to a 20 meter DEM., which clearly misinterprets the continuous surface producing an insufficient description of the terrain. The true peaks and troughs can become exaggerated. Producing a low resolution DEM from high density source data does not represent the terrain as well as a higher resolution DEM (Figure 2), which better represents the terrain (Liu, 2008). Using the rule put forth by Hengl in Equation (1), a transect with average horizontal spacing of measured points equaling 5 meters, a DEM size of 2.5 meters is recommended. However, the minimum spacing between the inflection points is 5 meters, so a DEM size of 5 meters is recommended (Figure 2). Further, this rule does not take into account the relative size of the DEM datasets and data processing.

Others have stated that DEM resolution should be no less than that of the original source data density (McCullagh, 1988; Florinksy, 1998, 2002; Liu, 2008):

$$GS = \sqrt{\frac{A}{N}} \tag{2}$$

where GS = grid size and A = total area containing N number of measured points. Finally, an optimal grid size for DEM development should be a function of both computational efficiency and accuracy (Hengl, 2006).

Current studies are now interested in determining methods of assimilating substantial high density LiDAR data sets into lower resolution finite element numerical models that simulate shallow water flow (Bates *et al.*, 2003). Past techniques of incorporating topographic data in storm inundation models were developed without prior knowledge of horizontal and vertical elevation variation scales. For example, mesh construction was performed *a posteriori* without knowledge or incorporation of raised features (i.e. roadbeds, levees, etc.) or other important vertical points into the model (Marks & Bates, 2000). Bates *et al.* (2003) reviewed a set of algorithms to define important topographic points in a DEM. The VIP method (Chen & Guevara, 1987) was determined to be the best fit for discretizing points for use in a finite element model. The study domain was discretized using the mesh generator Cheeseymesh (Horritt, 2000) with points determined by the VIP method. This mesh was compared to a mesh independent of topography (i.e. the mesh nodes were placed for numerical stability rather than for high topographic accuracy) developed by Marks and Bates (2000). It was found that the new mesh better represented the topography and differences of several meters between the two meshes were present. Also, the study indicated that determining topographically significant points is important in capturing correct flow physics.

It can be concluded that an optimal combination of the two main parameters in DEM construction, interpolation scheme and grid size, is not consistent in published literature or in practice. Also, a there is an absence of research in the literature that examines how mesh resolution, in terms of capturing significant topographic elevations, affects hydrodynamic models governed by the shallow water equations; in particular shallow water finite element models that discretize the domain with triangular finite elements (Dietsche *et al.*, 2007).

In practice, a raster DEM is generated based on bare earth LiDAR and interpolated to nodes on the linear finite element mesh. First, this study aims to determine the relative error (RMSE) between using the bare earth LiDAR points themselves and bare earth-derived DEMs at varying scales. Second, this paper provides a basis for determining a linear finite element mesh resolution based on the topographic data available from bare earth LiDAR. Third, a recommendation is made on the appropriate size of the DEM based on the target finite element mesh resolution.

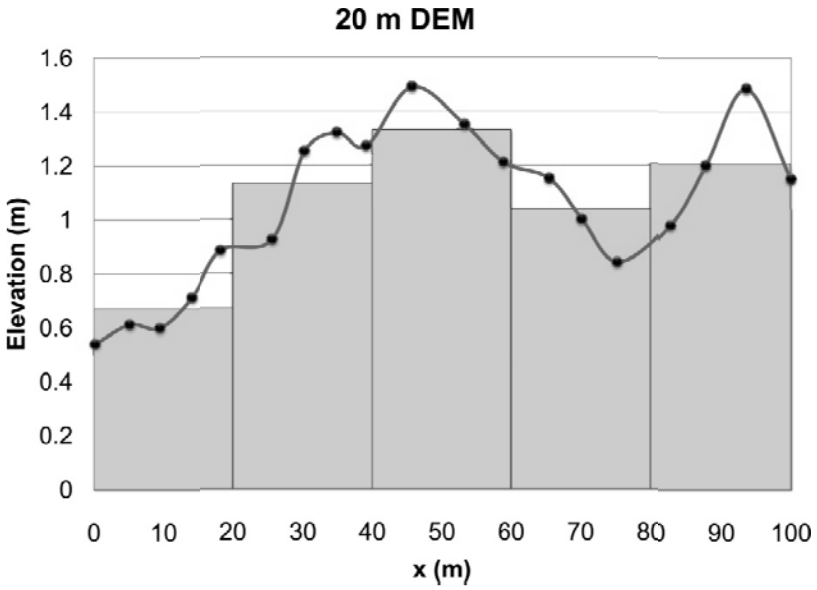

Figure 1 Plot with a set of measured elevation points (black points) along a transect (black curve) and the measured data resampled to a 20 meter DEM (gray rectangles) (Hengl, 2006).

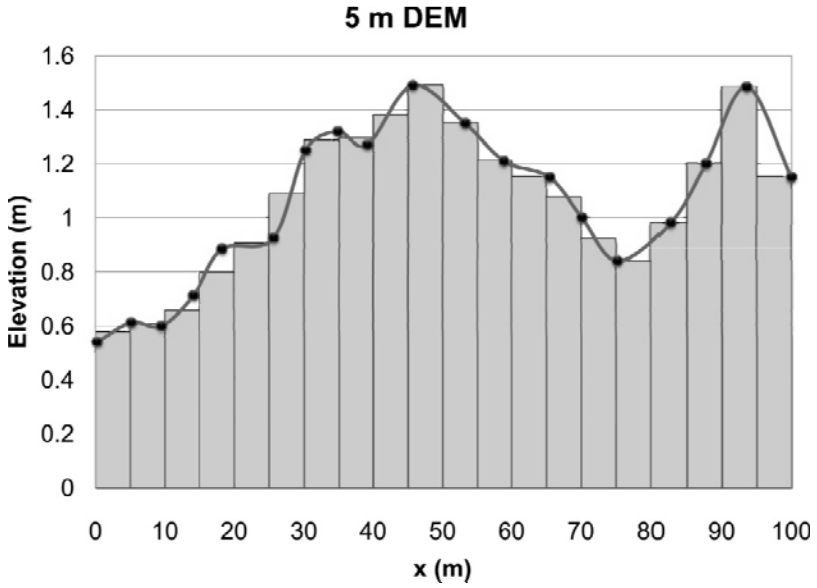

Figure 2 Plot of a set of measured elevation points (black) along a transect (red) and the measured data resampled to a 5 meter DEM grid (Hengl, 2006).

2. MATERIALS AND METHODS

2.1. Study Area

The study area is located in Jackson County, Mississippi (30°21'49''N 88°23'31''W). Jackson County is home to the Pascagoula River, which drains into the northern Gulf of Mexico. The land use/land cover of the area includes largely forested regions, with some farming and residential areas. Marshlands, wetlands and urban land are predominately found along the majority of the coastline, but dense forest occupies most of the floodplain. The topography is generally rolling with moderate relief (Oldham & Rushing, 1970; Slack, 1991; Strom, 1998).

2.2. Data Collection

LiDAR source data was acquired for Jackson and Hancock County, Mississippi from the Mississippi GIS Department. Data acquisition and processing was performed by EarthData International, LLC. The source data covers approximately 727 square miles and was collected at a nominal point spacing of five meters. The data collected was obtained using the Lecia ALS-50 LiDAR system along with an inertial measuring unit (IMU) and a frequency GPS receiver. It is equipped with a 50 kHz thermal infrared laser that can measure ground point spacing of one to eight meters. The data was acquired between February 25 and March 12, 2005. The specifications of the ALS-50 LiDAR system are listed in Table 1.

Using proprietary software, non ground point features were removed from the point cloud resulting in a bare earth LiDAR dataset. Both .las and xyz ASCII files were delivered. For Jackson county an accuracy assessment of the bare earth points resulted in a RMSE of 0.075 meters (7.5 cm) yielding an accuracy of +/- 14.7 cm using the following relationship defined by FEMA (FEMA, 2003):

$$Accuracy_z = 1.96 \times RMSE_z \tag{3}$$

where $RMSE_z$ is from the LiDAR report for bare earth points.

Table 1 Hancock & Jackson County LiDAR sensor parameters

Sensor Collection Parameters	
Flying Height	3,657 meters AMT
Target Airspeed	150 knots
Laser Pulse	29,900 Hz
Field of View	45 Degrees
Scan Rate	17 Hz
Average Swath Width	3,100 meters
Post Spacing	5 meters

2.3. Selection of Test Sites & Data Processing

Three test sites located in coastal Jackson County were chosen for an accuracy assessment (Figure 3). The methods presented are consistent, unless otherwise noted, for each of the three test sites. Each test site was chosen to encompass a range of typical coastal land cover. The first test site covers a forested region and small urban development (Figure 4). The second test site is located in a marsh area found between the East and West Pascagoula inlet (Figure 5) and the third is a developed, urban, area (Figure 6).

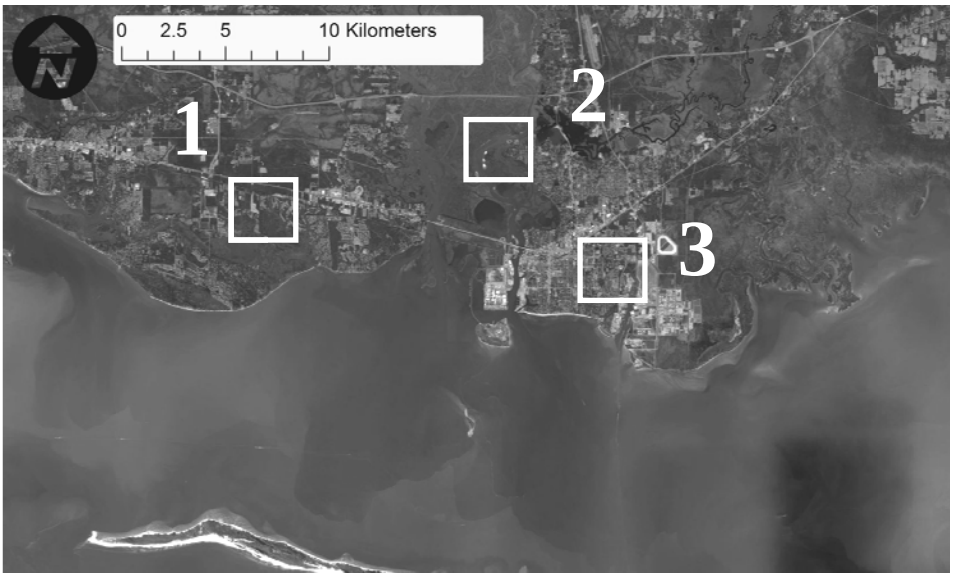

Figure 3 Pascagoula River, MS with box insets representing accuracy testing areas.

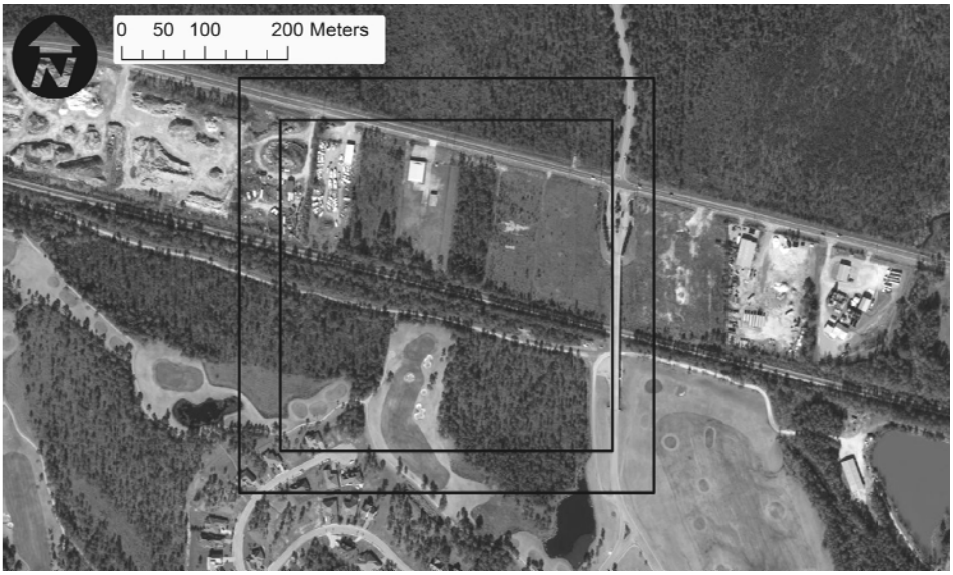

Figure 4 Test site 1

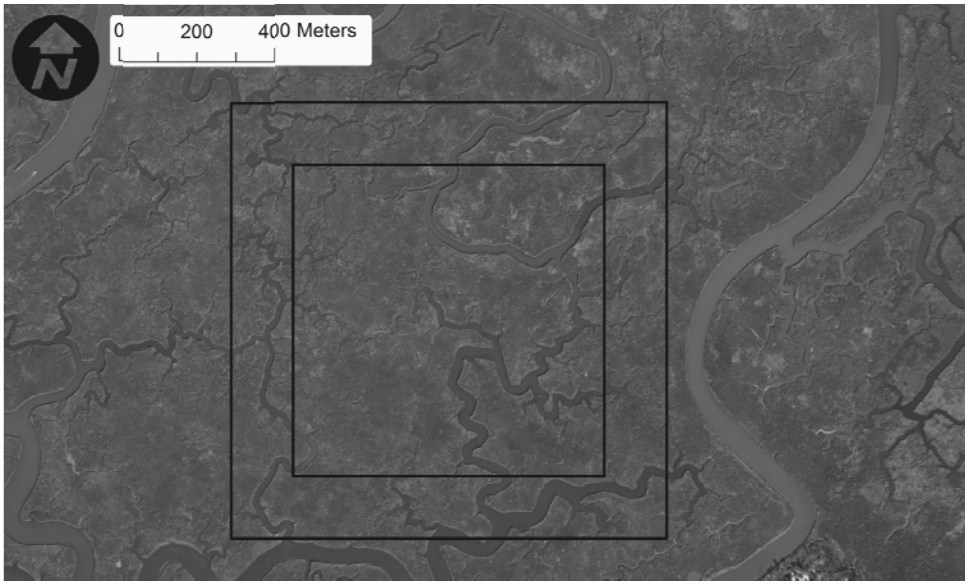

Figure 5 Test site 2

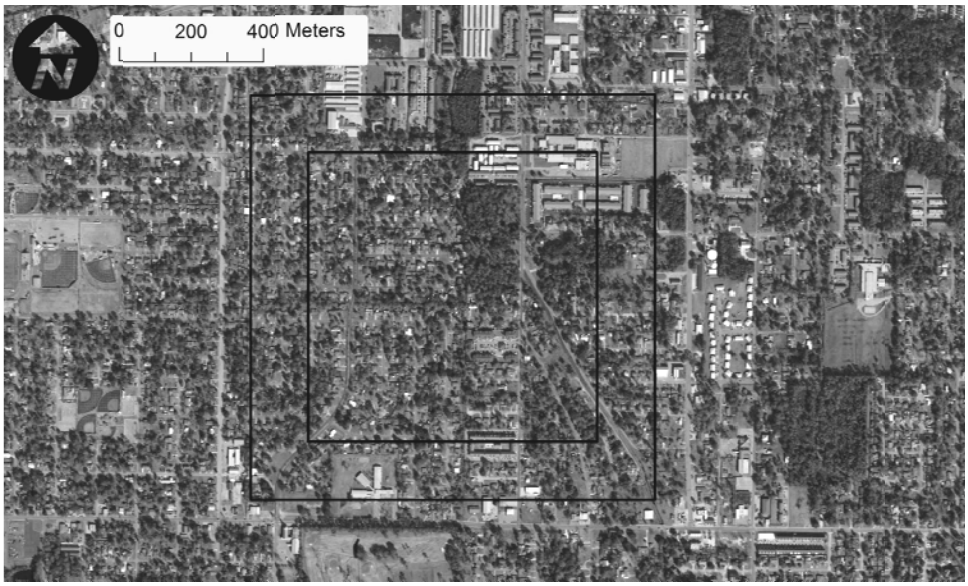

Figure 6 Test site 2

For each site, inner and outer boundaries were constructed. For test site 1, the outer boundary is 500 meters x 500 meters and the inner boundary is offset by 50 meters. Test Sites 2 and 3 are bounded by an 1120 meter by 1120 meter outer boundary and a 800 x 800 meter inner boundary (offset of 160 meters). The bare earth points were clipped to both boundaries as well to the transition zone. The transition zone was constructed to reduce edge effects. In other words, to properly obtain an elevation value at a mesh node along the inner boundary, the source elevation data points must be present around all directions of the mesh node. If the transition zone was removed, additional error would be included for mesh node along the boundary due to a lack of source data points. For the interior domain, the LiDAR points were randomly sub-divided into two datasets. The first dataset, termed the

training dataset, includes 90% of the points; the second, the test dataset, includes the remaining 10%. The ratio of training to test datasets yields enough to test the quality of the processed data without degrading the LiDAR data itself (Bater & Coops, 2009). The training dataset was used to generate the DEMs and finite element meshes, whereas the test dataset was used to assess vertical errors in elevation. Table 2 shows the number of LiDAR points for each test site and the average point spacing located inside the interior boundary.

It is important to note that this research was not intended to examine the geodetic accuracy of the collected bare earth LiDAR dataset. The focus is on examining how interpolation functions as well as linear triangular elements and raster DEMS predict and/or represent the vertical component of the source data. This method is similar to that employed by Bater & Coops (2009).

Table 2 Statistics of LiDAR for all test sites

Test Site No.	Name	Outer Area (km2)	Inner Area (km2)	No. Training Pts.	No. Test Pts.	Avg. Pt. Spacing (m)
1	Mixed	0.25	0.16	9 350	1 309	3.87
2	March	1.25	0.64	37 751	4 560	4.11
3	Urban	1.25	0.64	34 465	3 829	4.61

2.4. Interpolation Methods

Based on published literature, three interpolation methods were selected for this study: linear, inverse distance weighted, and natural neighbor. These methods are easily employed by the software program SMS 10.1 (Aquaveo LLC, 2010).

Linear interpolation is the most widely used mathematical representation of a DEM surface due to its simplicity and practicability (Zhu *et al.*, 2005). When using a TIN model, rather than a regular grid DEM, the surface of the TIN triangles, or elements, is a 3D surface in which a linear plane connects the three vertices, or nodes. However, with a regular grid DEM, a linear model only represents the surface in the X and Y direction, not the Z direction. To compute an unknown elevation value at a point surrounded by points with known elevation values, a linear interpolation first triangulates the known points to form a temporary TIN using a Delaunay triangulation scheme. Because the TIN surface is assumed to vary linearly across the triangle, the TIN describes a piecewise linear surface. For a triangle, the equation of the place is defined by three nodes of known elevations:

$$Ax + By + Cz + D = 0 \tag{4}$$

where *A, B, C,* and *D* are computed by the nodal locations $(x_1, y_1, z_1), (x_2, y_2, z_2), (x_3, y_3, z_3)$.

$$
\begin{aligned}
A &= y_1\left(z_2 - z_3\right) + y_2\left(z_3 - z_1\right) + y_3\left(z_1 - z_2\right) \\
B &= z_1\left(x_2 - x_3\right) + z_2\left(x_3 - x_1\right) + z_3\left(x_1 - x_2\right) \\
C &= x_1\left(y_2 - y_3\right) + x_2\left(y_3 - y_1\right) + x_3\left(y_1 - y_2\right) \\
D &= -Ax_1 - By_1 - Cz_1
\end{aligned} \tag{5}
$$

Rearranging terms, the equation of the plane can be represented as:

$$
z\left(x, y\right) = -\frac{A}{C}x - \frac{B}{C}y - \frac{D}{C} \tag{6}
$$

where *z(x,y)* is the elevation function at coordinates *x* and *y*. Solving (6) for a point located inside triangle ABC yields an elevation value linearly interpolated from nodes ABC (Aquaveo, 2007b).

IDW is based on the assumption that the target point being predicted should be influenced more by its closest points rather than points more distant (ESRI, 2008). The following expression, Shepard's equation, is the simplest expression for IDW interpolation (Shepard, 1968; Aquaveo, 2007a):

$$
z\left(x, y\right) = \sum_{i=1}^{N} w_i z_i \tag{7}
$$

where N is the number of known input points, w_i is the weighting function and z_i is the value of point i. For this project, $i = 3$, the three closest points. SMS 10.1 uses the following weighting function:

$$
w_i = \frac{\left[\frac{R - d_i}{Rd_i}\right]^2}{\sum_{i=1}^{N}\left[\frac{R - d_i}{Rd_i}\right]^2} \tag{8}
$$

where R is the distance from the most distant scatter point and d is the distance from the target point to the input point.

Natural neighbor interpolation looks for the closest points to an unknown point and applies weights based on proportionate areas. Similar to the linear interpolation method, the known points are triangulated using the Delaunay triangulation method. Next, a Voronoi (or Thiessen) polygon is constructed for each point using the circumcircles of the Delaunay triangles. The Voronoi polygon represents the region of influence around the unknown point. Therefore, each point has an associated area, which is a polygon that defines the boundaries of strength of the point.

To estimate a value at point P, it is inserted as a new point resulting in a new triangulation. Therefore, a new network of Voronoi polygons are created, in which P has its own area of influence that overlaps with the Voronoi region of its neighbors. This determines how P fits into the existing points. The value of P is calculated based on the portion of the area that it "borrows" from each neighboring polygon in the previous network. For example, if the areas of the contributing polygons are $A_i, i = 1,2 \ldots, N$, then the relative portion borrowed from each of the original areas are (Sibson, 1981):

$$\lambda_i = \frac{A_i}{\sum_{i=1}^{N} A_i} \tag{9}$$

Therefore, the value at P (z_p) is the summation of the relative portion of each contributing polygon (λ_i) multiplied by the value of its point z_i:

$$Z_p = \sum_{i=1}^{N} \lambda_i Z_i \tag{10}$$

2.5. DEM and Finite Element Mesh Generation

In all, five DEMs were produced for Test Site 1, and eight for Test Site 2 and 3. All sites included DEMs at resolutions of 20, 10, 5, 2.5, and 1.25 meters and Test Site 2 and 3 also included grid sizes of 40, 80, and 160 meters. The source dataset for all DEMs were the training datasets merged with the transition (edge) dataset. ESRI ArcGIS 10 (ESRI, 2011a) was used to generate all DEMs. The method for each test site is similar to that of Medeiros *et al.* (2011) where the terrain dataset (TDS) within ArcGIS was utilized. See Medeiros *et al.* (2011) and ESRI (2011b) for a detailed description of a TDS. Once a terrain was compiled, the Terrain to Raster tool in the 3D Analyst Toolbox was used, with a linear interpolation, to convert the terrain to a raster DEM.

Similar to that of the DEMs, 5 structured finite element meshes (FEMs) for Test Site 1 and eight for Test Site 2 and 3 were generated. The elements within the mesh were chosen to be equilateral to best depict a regular interval and perfect triangulation for description of topography. Equilateral elements are also the most numerically stable when used in finite element models. For each test site, the largest mesh, 20 meters for test site one (Figure 7), and 160 meters for test sites two and three are refined down to 1.25 meters in element edge length. Refinement splits the edge length in half, and the entire element into 4 sub-elements as depicted in Figure 8.

The source elevation data were the training and edge dataset, 5 meter and 10 meter DEM for the finite element meshes. All three were interpolated onto each finite element mesh at each test location using the three interpolation schemes outlined previously.

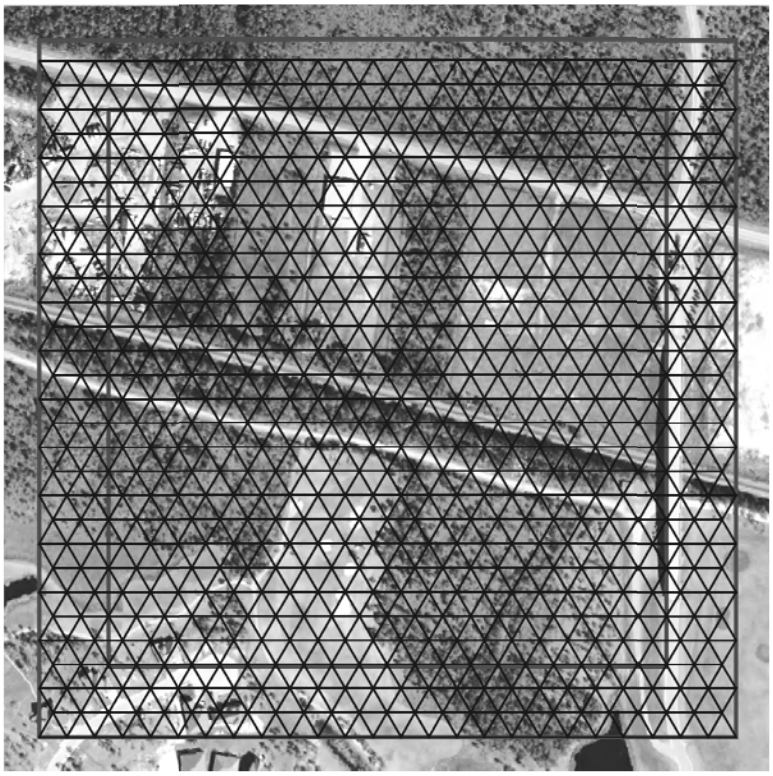

Figure 7 20m structured mesh for test site one.

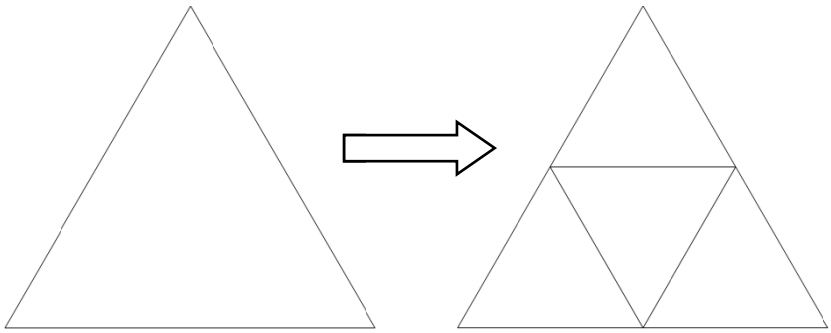

Figure 8 Refine mesh element (Element is split by four)

2.5. Accuracy Analysis

Using all DEMs and FEMs for each test site generated using the training dataset, the test dataset points were used to compare the accuracy between all representative surfaces. For each DEM and FEM, vertical errors were computed for each point in the test dataset using the root mean square error (RMSE) approach:

$$RMSE = \sqrt{\frac{\sum_{i=1}^{N} \left(M_z(x,y) - I_z(x,y) \right)^2}{N}} \quad (11)$$

where $M_z(x,y)$ is the measured (LiDAR) elevation and $I_z(x,y)$ is the predicted (interpolated) elevation value at coordinate *x,y*. RMSE is commonly used to measure the precision of DEMs derived from points using interpolation functions (Desmet, 1997). RMSE is a measure of the global accuracy of the surface in which the interpolated value disagrees from the measured value. As stated previously, it is important to note that the elevation value, when comparing to the DEMs, is that of the center of the DEM grid cell, while the test points are unlikely to occur at or near the center. This results in some additional error when comparing the test points to the DEM surface (Bater & Coops, 2009).

3. RESULTS AND DISCUSSION

Elevation error was computed in terms of RMSE for vertical differences in interpolated values across the test dataset for three test sites located in Pascagoula, MS. RMSE for each FEM and DEM at the locations of each test point in the test dataset are presented. Table 3 presents the RMSE across all finite element meshes and DEMs which obtained elevations from the training dataset using a linear interpolation. Site 1 includes FEMs and DEMs of size 20 to 1.25 meters. Sites two and three include a larger number of element and grid size from 160 to 1.25 meters. In order to capture the features within test site one, only the low end of the size spectrum was chosen.

The greatest range of error is present in test site three, both in the FEM and DEM representation. Test site three is the urbanized area east of the east Pascagoula inlet (Figure 6). The area is characterized with heavy manmade structures. LiDAR returns on these areas are removed from the raw point cloud in the generation of the bare earth points, thus leaving artificial fissures in the bare earth dataset. This results in larger error within test site three, as well as test site one, when compared to site two. Site two, as expected, has lower error in all sizes, regardless of the low point density.

Generally, both source elevation datasets perform similarly at the larger scales (20 meters and above). For all sizes and sites, the FEMs have lower RMSE than the DEMs, with larger differences found on the smaller scales (10 meters and lower). In all cases, the finite element mesh outperforms the gridded raster DEM; however as Bater and Coops (2009) point out, higher resolution DEMs may perform better as a result of the test points occurring at decreased distances from the grid cell centers. Thus, linear elements have an advantage, particularly due to the 3D nature of the polygon's surface.

The results signify that grid and element mesh resolution is an important factor that can significantly affect overall global accuracy in elevation. It is not uncommon to model any of the test sites with 160 meter, or even larger, elements

which would result in ~20% increase in error from that of the lower resolutions. As the resolution increases, error decreases showing better fit to the source data (Figure 9).

Table 4 presents RMSE across the finite element meshes using the 5 meter DEM and 10 meter DEM as the source elevation data. The meshes with elevations derived from the 5 meter DEM perform better than the meshes developed from the 10 meter DEM at element edge lengths of 5 meters and less. Scales larger than 5 meters, both sets of meshes are generally comparable. At test site two and three, all three 20 meter finite element meshes resulted in similar RMSE.

RMSE for the three interpolating functions (linear, IDW, and NN) used to obtain nodal elevations onto the finite element meshes using the 5 meter and 10 meter DEMs are presented in Table 5 and Table 6 for test site two and three, respectively. Linear and NN generally perform well and are similar in all cases with IDW yielding greater error for most grid sizes. IDW had larger error in areas where LiDAR returns were removed due to manmade features or water.

Table 3 RMSE for all test sites with a linear interpolation of the training dataset onto the finite element meshes and DEMs

	Training to Finite Element Mesh - RMSE (cm)			**Training to DEM - RMSE (cm)**		
Size (m)	**Site 1**	**Site 2**	**Site 3**	**Site 1**	**Site 2**	**Site 3**
1.25	9.48	3.06	11.43	9.70	8.78	11.65
2.5	9.46	3.88	11.45	10.29	8.9	11.84
5	10.00	5.89	11.64	11.95	9.42	13.02
10	12.10	8.65	13.82	16.43	10.67	16.19
20	17.30	11.37	19.96	24.37	13.22	21.61
40	-	14.13	27.06	-	16.09	31.4
80	-	16.94	31.42	-	17.88	36.43
160	-	18.73	50.72	-	20.88	41.47

Table 4 RMSE for all sites with a linear interpolation of the 5 meter DEM and 10 meter DEM interpolated onto the finite element meshes

	5m DEM to Finite Element Mesh - RMSE (cm)			10m DEM to Finite Element Mesh - RMSE (cm)		
Size (m)	**Site 1**	**Site 2**	**Site 3**	**Site 1**	**Site 2**	**Site 3**
1.25	10.33	6.35	11.77	13.15	9.04	14.47
2.5	10.32	6.46	11.80	13.14	9.04	14.48
5	10.74	6.97	12.04	13.20	9.07	14.58
10	12.26	8.53	14.06	13.76	9.38	15.19
20	17.00	11.11	19.70	16.96	11.05	19.71
40	-	13.81	26.74	-	13.60	26.49
80	-	16.67	30.88	-	16.49	30.61
160	-	18.71	48.99	-	18.52	48.43

Table 5 RMSE for site two using linear, IDW, & NN interpolation

	5m DEM to Finite Element Mesh - RMSE (cm)			10m DEM to Finite Element Mesh - RMSE (cm)		
Size (m)	**Linear**	**Inverse Distance Weighted***	**Natural Neighbor**	**Linear**	**Inverse Distance Weighted***	**Natural Neighbor**
1.25	6.35	7.91	6.11	9.04	10.93	8.93
2.5	6.46	1.83	6.22	9.04	10.68	9.04
5	6.94	8.62	6.86	9.07	10.62	6.86
10	8.53	9.31	8.55	9.38	11.2	9.3
20	11.11	11.49	11.18	11.05	11.88	11.12
40	13.81	13.96	13.89	13.60	13.89	13.72
80	16.67	16.59	16.77	16.49	16.39	16.57
160	18.71	18.99	18.96	18.52	18.66	18.66

*****Using three closest points

Table 6 RMSE for test three using linear, IDW, & NN interpolation

	5m DEM to Finite Element Mesh - RMSE (cm)			10m DEM to Finite Element Mesh - RMSE (cm)		
Size (m)	**Linear**	**Inverse Distance Weighted***	**Natural Neighbor**	**Linear**	**Inverse Distance Weighted***	**Natural Neighbor**
1.25	11.77	13.67	11.80	14.47	16.91	14.08
2.5	11.80	14.10	11.75	14.48	17.00	14.08
5	12.04	14.44	12.09	14.58	17.33	14.11
10	14.06	15.26	14.08	15.19	18.16	15.07
20	19.70	20.75	19.97	19.71	21.46	20.07
40	26.74	27.33	26.89	26.49	25.67	26.82
80	30.88	32.39	30.88	30.61	29.58	31.06
160	48.99	52.67	50.09	48.43	42.17	50.09

***Using three closest points

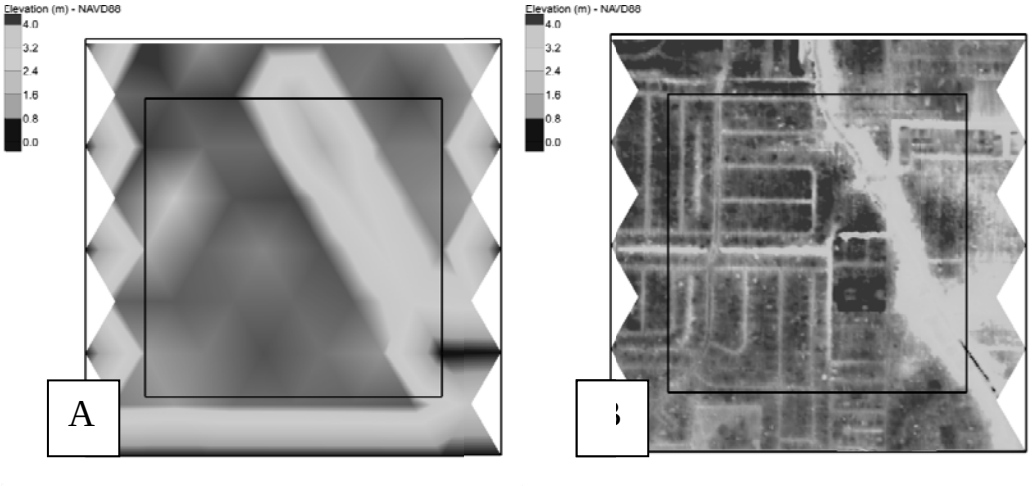

Figure 9 Finite element mesh of site 3 at a element edge length resolution of A) 160 meters and B) 2.5 meters

4. CONCLUSIONS

The results obtained in this research confirm the validity of using a DEM as an elevation source for a finite element mesh, as current practice dictates. Software tools popular in geospatial analysis such as ESRI ArcGIS, Global Mapper and Aquaveo's finite element meshing tool, SMS (Surface Water Modeling System), are fine tuned in working with raster DEM products rather than irregular spaced points.

Secondly, results show that the Shannon-Nyquist theorem can be applied to terrain grid resolution. It is shown that having a DEM or finite element mesh size

less than half the data density yields no significant decrease in RMSE. Also, it is found that a DEM size can be related to element size. It is shown that if an element size is 20 meters, a 10 meter DEM should suffice, rather than using the bare earth or a higher resolution DEM as the elevation source. Interpolating the 10 meter DEM to the 20 meter finite element resulted in similar RMSE as interpolating the 5 meter DEM and bare earth LiDAR to the finite element mesh. Careful consideration should be exercised when choosing a DEM grid size or finite element mesh size with respect to data capacity and computation resources available.

Further, between three interpolating routines (linear, IDW, and NN), linear and NN performed best, with IDW resulting in increased error when non bare-earth features are removed. Linear is preferred over NN due to its simple parameterization and efficient algorithm. Also, linear interpolation performs faster than that of IDW or NN.

Since this study uses pure equilateral elements and does not include significant linearly raised features, future work should be conducted to assess how including vertical features and non-equilateral elements affect topographic elevation error.

It is evident that additional work should be conducted to make more firm recommendations on the relation, in topographic accuracy, between DEM and finite element mesh grid size.

5. ACKNOWLEDGEMENTS

This study is funded in part by Award number NFWMD-08-073 from the Northwest Florida Water Management District (NWFWMD). The views expressed herein are those of the authors and do not necessarily reflect the views of the NWFWMD. The authors wish to thank Stephen Medeiros and David Coggin for their guidance and assistance.

6. REFERENCES

Ali, T. (2004). *On the selection of an interpolation method for creating a terrain model (TM) from LIDAR data.* Paper presented at the American Congress on Surveying and Mapping (ACSM) Conference 2004, Nashville, TN, U.S.A.

Anderson, E. S., Thompson, J. A., & Austin, R. E. (2005). LIDAR data density and linear interpolator effects on elevation estimates. *International Journal of Remote Sensing, 26*(18), 3889-3900.

Aquaveo. (2007a). SMS: Inverse Distance Weighted Interpolation, from http://www.xmswiki.com/xms/SMS:Inverse_Distance_Weighted_Interpolation

Aquaveo. (2007b). SMS: Linear Interpolation, from http://www.xmswiki.com/xms/SMS:Linear_Interpolation

Aquaveo LLC. (2010). Surface-water Modeling System (Version 10.1). Provo, Utah. Retrieved from http://xmswiki.com/xms/SMS:SMS,

Bacopoulos, P. (2009). *Estuarine Influence on Tidally Driver Circulation in the South Atlantic Bight.* Ph.D., University of Central Florida, Orlando, FL.

Bater, C. W., & Coops, N. C. (2009). Evaluating error associated with lidar-derived DEM interpolation. *Journal of Computers and Geosciences, 35*(2), 289-300.

Bates, P. D., Marks, K. J., & Horritt, M. S. (2003). Optimal Use of High-Resolution Topographic Data in Flood Inundation Models. *Hydrological Processes, 17*, 537-557. doi: 10.1002/hyp.1113

Blain, C. A., Westerink, J. J., & Luettich, R. A. (1994). The influence of domain size on the response characteristics of a hurricane storm surge. *Journal of Geophysical Research, 99*(C9), 18,467-418,479.

Bunya, S., Dietrich, J. C., Westerink, J. J., Ebersole, B. A., Smith, J. M., Atkinson, J. H., . . . Roberts, H. J. (2010). A high-resolution coupled riverine flow, tide, wind, wind wave, and storm surge model for southeastern Lousiana and Mississippi. Part I: Model development and validation. *Monthly Weather Review, 128*(345-377).

Chen, Z.-T., & Guevara, J. A. (1987). *Systematic Selection of Very Important Points (VIP) From Digital Terrain Model For Constructing Triangular Irregular Networks.* Paper presented at the AUTO-CARTA 8, Falls Church, USA.

Coggin, D. (2011). A digital elevation model for Franklin, Wakulla, and Jefferson Counties. *Florida Watershed Jounral, 4*(2), 5-10.

Desmet, P. J. J. (1997). Effects of interpolation errors on the analysis of DEMs. *Earth Surface Processes and Landforms, 22*, 563-580.

Dietsche, D., Hagen, S. C., & Bacopoulos, P. (2007). Storm surge simulations for Hurricane Hugo (1989): On the significance of inundation areas. *Journal of Waterway, Port, Coastal, and Ocean Engineering, 133*(3), 183-191.

ESRI. (2008). ArcGIS: The complete enterprise GIS Retrieved 04-25-2011, 2011, from http://www.esri.com/software/arcgis/

ESRI. (2011a). ArcGIS Desktop: Release 10. Redlands, CA: Environmental Systems Research Institute.

ESRI. (2011b). ArcGIS Resource Center, from http://resources.arcgis.com/

FEMA. (2003). Appendix A, Guidance for aerial mapping and surveying, *Guidelines and Specifications for Flood Hazard Mapping Partners*: Federal Emergency Management Agency.

Florinksy, I. V. (1998). Combined analysis of digital terrain models and remotely sensed data in landscape investigations. *Progress in Physical Geography, 22*(1), 33-60.

Florinksy, I. V. (2002). Errors of signal processing in digital terrain modelling. *International Journal of Geographical Information Science, 16*(5), 475-501.

Gao, J. (1997). Resolution and accuracy of terrain representation by grid DEMs at a micro-scale. *International Journal of Geographical Information Science, 11*(2), 199-212.

Hengl, T. (2006). Finding the right pixel size. *Computers & Geosciences, 32*(9), 1283-1298. doi: DOI 10.1016/j.cageo.2005.11.008

Horritt, M. (2000). Development of physically based meshes for two dimensional models of meandering channel flow. *International Journal of Numerical Methods in Engienering, 47*(2019-2037).

Kienzle, S. (2004). The Effect of DEM Raster Resolution on First Order, Second Order and Compound Terrain Derivatives. *Transactions in GIS, 8*(1), 83-111.

Kubik, K., & Botman, A. G. (1976). Interpolation accuracy for topographic and geological surfaces. *ITC Journal, 2*(236-274).

Li, Z., Zhu, Q., & Gold, C. (2005). *Digital Terrain Modeling: Principles and Methodology*. London, New York, and Washington, D.C.: CRC Press.

Liu, X. (2008). Airborne LiDAR for DEM generation: some critical issues. *Progress in Physical Geography, 32*(1), 31-49.

Lloyd, C. D., & Atkinson, P. M. (2002). Deriving DSMs from LiDAR data with kriging. *International Journal of Remote Sensing, 23*(12), 2519-2524.

Lynch, D. R. (1983). Progress in hydrodynamic modeling, review of U.S. contributions. *Reviews of Geophysics and Space Physics, 21*(3), 741-754.

Marks, K., & Bates, P. D. (2000). Integration of high resolution topographic data with floodplain flow models. *Hydrological Processes, 14*, 2109-2122.

Maune, D. F. (2007). *Digital Elevation Model Technologies and Applications: The DEM Users Manual* (2 ed.). Bethesda, Maryland: American Society for Photogrammetry and Remote Sensing.

McCullagh, M. J. (1988). Terrain and surface modelling systems: theory and practice. *Photogrammetric Record, 12*(72), 747-779.

Medeiros, S. C., Ali, T., & Hagen, S. C. (2011). Development of a seamless topographic/bathymetric digital terrain model for Tampa Bay, Florida. *Photogrammetric Engineering & Remote Sensing, In Press*.

Oldham, M. B. J., & Rushing, J. W. (1970). Water Resources Planning for Pascagoula Basin. *Journal of Waterways and Harbors Division, Proceedings of the American Society of Civil Engineers, 96*(WWI), 65-85.

Shannon, C. E. (1949). *Communication in the presence of noise.* Paper presented at the Institute of Radio Engineers.

Shepard, D. (1968). *A two-dimensional interpolation function for irregularly-spaced data.* Paper presented at the ACM National Conference.

Sibson, R. (1981). A brief description of natural neighbor interpolation *Interpreting Multivariate Data* (pp. 21-36). Chichester: John Wiley.

Slack, L. J. (1991). Mississippi Stream Water Quality: National Water Summary 1990-91 *United States Geological Survey Water Supply Paper 2400* (pp. 343-350).

Strom, E. W. (1998). The Pascagoula River Basin. *The Rivers of Mississippi* Retrieved 08/11/2011, 2011, from http://ms.water.usgs.gov/ms_proj/eric/pasca.html

Su, J., & Borke, E. (2006). Influence of vegetation, slope and lidar sampling angle on DEM accuracy. *Photogrammetric Engineering & Remote Sensing, 72*(11), 1265-1274.

Westerink, J. J., Luettich, R. A., Baptista, A. M., Scheffner, N. W., & Farrar, P. (1992). Tide and storm surge predictions using a finite element model. *Journal of Hydraulic Engineering, 118*, 1373-1390.

Westerink, J. J., Luettich, R. A., & Muccino, J. C. (1994). Modeling tides in the western North Atlantic using unstructured graded grids. *Tellus, 46A*, 178-199.

Zhu, C., Shi, W., Li, Q., Wang, G., Cheung, T. C. K., Dai, E., & Shea, G. Y. K. (2005). Estimation of average DEM accuracy under linear interpolation considering random error at the nodes of a TIN model. *International Journal of Remote Sensing, 26*(24), 5509-5523.

View publication stats